Acta Mech 227, 1969–1982 (2016)
DOI 10.1007/s00707-016-1615-4

ORIGINAL PAPER

H. Khajehsaeid · S. Reese · J. Arghavani · R. Naghdabadi

# Strain and stress concentrations in elastomers at finite deformations: effects of strain-induced crystallization, filler reinforcement, and deformation rate

Received: 12 September 2015 / Revised: 9 December 2015 / Published online: 6 April 2016


**Abstract** Strain and stress concentrations are studied for elastomers at finite deformations. Effects of strain-induced crystallization, filler reinforcement and deformation rate are also investigated, and micromechanical descriptions are provided for the observed results. A simple problem is subjected to finite element simulations to show the results evidently. Material parameters are obtained from experimental tests conducted on standard tensile samples of filled and unfilled natural rubber (NR) as well as styrene–butadiene rubber (SBR) as crystallizing and non-crystallizing rubbers, respectively. In all simulations, the strain concentration factor $K_E$ is shown to decrease monotonically where the reduction is more apparent as the filler content increases. At enough large stretches, $K_E$ is higher for filled NRs compared to the unfilled NR which is not the case for SBR. The stress concentration factor $K_S$ rises sharply by deformation of the samples. At large stretches, in the case of SBR, filler reinforcement only shifts the maximum value of $K_S$ to a lower level of strain, while in the case of NR, it reduces $K_S$ significantly. It is concluded that $K_S$ can rise from its theoretical value remarkably which should be noticed in design purposes particularly for crystallizing elastomers. Furthermore, the effect of deformation rate is investigated employing a visco-hyperelastic constitutive law along with an associated VUMAT in ABAQUS/Explicit. It is observed that, at high deformation rates, $K_E$ decreases. Despite the reduction in strain concentration, $K_S$ would be higher which is not desired in design of mechanical parts.

## 1 Introduction

Elastomers consist of long cross-linked polymeric chains with high flexibility and mobility in a three-dimensional network configuration. The flexibility and mobility of the chains are associated with the most outstanding property of these materials—i.e., high deformability—from which the terminology of "Elastomer" has been derived [1]. Stress can cause molecular chains of elastomers to adopt an extended configuration, and upon removal of the stress the chains retract to their initial coiled configuration [2].

H. Khajehsaeid (✉)
School of Engineering–Emerging Technologies, University of Tabriz, Tabriz, Iran
E-mail: Khajehsaeid@Tabrizu.ac.ir
Tel.: +98 41 33393880
Fax: +98 41 33294626

S. Reese
Institute of Applied Mechanics, RWTH–Aachen University, Aachen, Germany

J. Arghavani · R. Naghdabadi
Department of Mechanical Engineering, Sharif University of Technology, Tehran, Iran

R. Naghdabadi
Department of Mechanical Engineering and Institute for Nano–Science and Technology, Sharif University of Technology, Tehran, Iran

Several engineering applications count on elastomeric materials, e.g., springs, bearings, dampers, belts and tires. In most applications, it is necessary to join elastomeric parts to rigid materials to be bolted to structural members. They are either adhered to metal parts by bonding during vulcanization [3,4] or by means of mechanical joints which necessitate introduction of holes, shoulders, grooves, etc. The elementary stress formulas are based on the members with constant cross sections or sections with gradual change of contour which are hardly ever attained in actual applications [5]. Introduction of holes, shoulders, grooves, nicks, etc. can modify distributions of strain and stress in mechanical parts and cause their localizations. Crack initiation and propagation in structures often occurs from stress and/or strain concentration sites where the local stress and/or strain exceeds a critical level [2,6].

In most studies, only the stress concentration factors are considered, while due to nonlinear mechanical behavior of elastomers, strain and stress distributions may differ significantly. Yang et al. [7,8] realized that, even for metals in three-dimensional stress states, stress concentration factor is different from strain concentration factor and Poisson's ratio affects strain concentration more than stress concentration.

Stress concentration factors can be determined analytically from the elasticity theory, computationally from the finite element method, and experimentally from strain gauges or photoelasticity methods. In recent decades, the universal availability and high efficiency of the finite element method has reduced the need for analytical and experimental methods and also explicit use of stress concentration factors [5].

Lindley [3] studied the strain concentrations at the corners of stretched rubber sheets under conditions of plane stress with focus on the effects of different shapes and size of the corners. Conveyor belts are typical applications in which thin rubbery sheets are stretched. Fukahori and Seki made numerical stress and strain analyses around spherical holes in elastomers. They also investigated the influence of adjacent holes on stress and strain distribution around a spherical hole [9]. Troyani et al. [10,11] analyzed effects of length of elements on stress concentration factor for rectangular sheets with circular hole at the center. They performed finite element analyses on thin elements of varying lengths in uniaxial tension and found that if the length is less than the width, the stress concentration factor available for elements of infinite length is of questionable accuracy. Elmukashfi and Kroon studied dynamic crack propagation due to strain and stress concentrations in rubbers using the finite element method. They obtained a minimum threshold stretch required for crack propagation [6].

In this paper, variations of strain and stress concentration factors with respect to the applied deformation are studied for elastomers. As a typical problem of local strain and stress concentration, a rectangular elastomeric sheet with circular hole at the center is analyzed numerically. To find out the probable effect of strain-induced crystallization on the distribution of strain and stress and consequently on concentration factors, the analysis is performed on a crystallizing rubber (NR) and a non-crystallizing one (SBR). Then, the effect of filler particles on the strain and stress concentration factors is investigated on both materials with focus on the micromechanical effects of fillers on the materials molecular network. Furthermore, the concentration factors have been analyzed for dynamic deformations from low to high strain rates over a wide range of strain to find out how, if at all, the deformation rate affects the distributions of strain and stress.

## 2 Strain and stress concentrations in elastomeric rectangular sheets with circular hole at the center: finite deformations

In order to investigate strain and stress distributions in elastomers at different levels of applied deformations, the typical problem of uniaxial tension of a rectangular sheet with circular hole at the center is considered in this section (Fig. 1). In the case of the linear elasticity theory, a two-dimensional stress distribution of a homogenous elastic body is a function of the body geometry and does not depend on the material properties. In this theory, for an infinite rectangular sheet with a small circular hole (compared with length and width of the sheet), the stress components are as follows [12]:

$$\begin{aligned}
\sigma_{rr} &= \frac{\sigma}{2}\left(1-\frac{R^2}{r^2}\right)+\frac{\sigma}{2}\left(1-\frac{4R^2}{r^2}+\frac{3R^4}{r^4}\right)\cos 2\theta,\\
\sigma_{\theta\theta} &= \frac{\sigma}{2}\left(1+\frac{R^2}{r^2}\right)-\frac{\sigma}{2}\left(1+\frac{3R^4}{r^4}\right)\cos 2\theta,\\
\tau_{r\theta} &= \frac{-\sigma}{2}\left(1+\frac{2R^2}{r^2}-\frac{3R^4}{r^4}\right)\sin 2\theta
\end{aligned} \tag{1}$$

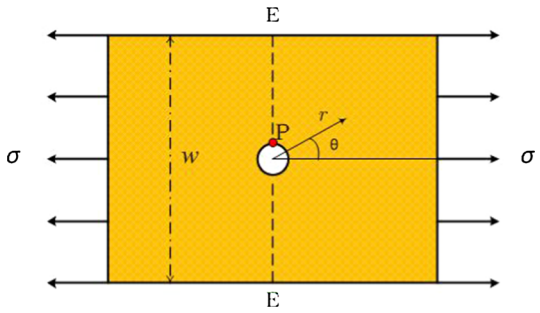


**Fig. 1** The *rectangular sheet* with *circular hole* at the center under uniaxial tension

where $R$ is the radius of the hole, $\sigma$ is the applied stress to the edges of the sheet, and $r$ and $\theta$ are the components of polar coordinates measured from the center of the hole. At the edge of the hole $r = R$, one obtains:

$$\begin{aligned} &\sigma_{rr} = 0, \\ &\sigma_{\theta\theta} = \sigma(1 - 2\cos 2\theta), \\ &\tau_{r\theta} = 0. \end{aligned} \tag{2}$$

The maximum stress at the hole edge occurs for $\theta = \frac{\pi}{2}, \frac{3\pi}{2}$. Therefore, the stress concentration factor for a finite sheet is calculated as ratio of the stress at critical point $P$ to the average stress at the cross section $EE$:

$$K_S = \frac{\sigma_{\theta\theta}|_P}{\sigma_{\theta\theta}^{ave}|_{EE}} = \frac{3\sigma}{\frac{\sigma w}{w-2R}}. \tag{3}$$

Regarding the nonlinear mechanical behavior of elastomers, the strain and stress concentration factors are expected to depend on the material properties and also vary with respect to the applied deformations even in a two-dimensional stress state. To see how, if at all, these factors vary, finite element analysis is performed on a rectangular sheet (160 × 120 mm) of unfilled natural rubber (NR) with a circular hole ($R = 3$ mm) at the center subjected to uniaxial tensile deformation. The ratio of the calculated nominal strain (Cauchy stress) at the critical point P to the average nominal strain (Cauchy stress) at the critical cross section (EE) is determined numerically to determine variations of the concentration factor $K_E(K_S)$ with respect to the applied strain. For the specific geometry considered in the numerical finite element analysis, using Eq. (3) one obtains:

$$K_S = \frac{3\sigma}{\frac{\sigma w}{w-2R}} = 2.85. \tag{4}$$

For numerical simulations, one requires to know material parameters of the material under study. Therefore, a quasi-static uniaxial tension test is conducted on a dumbbell-shaped standard tensile sample to obtain the stress–strain curve. The test is continued till rupture of the sample to obtain breakage strain ($\varepsilon_{break}$) of the material. The primary loading curve as the most critical one is used to determine the material parameters. Due to the Mullins effect, in the upcoming loadings some amount of softening would appear which partially moderates the strain and stress concentrations. The experimental curve should be fitted by means of a nonlinear hyperelastic model which gives satisfactory results in the considered large stretches [13]. Arruda–Boyce [14], Pucci–Saccomandi [15] and Exp-Ln [16] hyperelastic models are examined as models which give reasonable results in different modes of deformation [17,18]:

$$W^{AB} = \mu\sqrt{N}\left[\beta\sqrt{\frac{I_1}{3}} + \sqrt{N}\ln\left(\frac{\beta}{\sinh\beta}\right)\right], \tag{5}$$

$$W^{PS} = -\frac{\mu}{2}J_m \ln\left(1 - \frac{I_1 - 3}{J_m}\right)) + C_2 \ln\left(\frac{I_2}{3}\right), \tag{6}$$

$$W_e^{Exp-Ln} = A\left[\frac{1}{a}\exp(a(I_1 - 3)) + b(I_1 - 2)(1 - \ln(I_1 - 2)) - \frac{1}{a} - b\right] \tag{7}$$

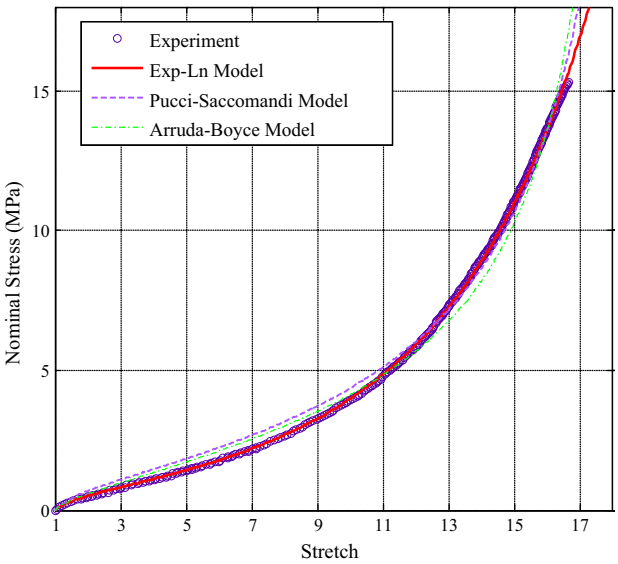


**Fig. 2** Stress–strain curve of the unfilled NR in uniaxial tension

**Table 1** Material parameters of different models for the unfilled NR

| Hyperelastic model | Material parameters |
|---|---|
| Arruda–Boyce | $\mu = 0.33$, $N = 121.3$ |
| Pucci–Saccomandi | $\mu = 0.311$, $J_m = 394.4$, $C_2 = 0.15$ |
| Exp-Ln | $A = 0.152$, $a = 0.0044$, $b = 0.05$ |

where $\mu$, $N$, $J_m$, $C_2$, $A$, $a$ and $b$ are material parameters. $\beta$, $I_1$ and $I_2$ are inverse Langevin function, the first and second invariants of the left Cauchy–Green deformation tensor $\mathbf{B}$, respectively. The equilibrium Cauchy stress tensor ($\boldsymbol{\sigma}^{equ}$) can be calculated as follows [19]:

$$\boldsymbol{\sigma}^{equ} = -p^e\mathbf{I} + 2\left(\frac{\partial W^e}{\partial I_1} + I_1\frac{\partial W^e}{\partial I_2}\right)\mathbf{B} - 2\frac{\partial W^e}{\partial I_2}\mathbf{B}^2 \tag{8}$$

where $p^e$ is a hydrostatic pressure and $\mathbf{I}$ is the second-order identity tensor. The experimental stress–strain curve along with the fitted curves is exhibited in Fig. 2, and the material parameters are reported in Table 1. It is observed that the Exp-Ln model gives a slightly better fitting. Moreover, its parameters have been shown to be related to the physical properties of the material molecular network, i.e., cross-link density and average length of chain segments; thus, by determination of the parameters from uniaxial tension data one can obtain reasonable results for other modes of deformation [17,18]. Consequently, in the rest of the paper we will utilize this model for our simulations.

It should be noted that there are some problems in fitting experimental data by hyperelastic models to find the parameter set accurately and uniquely. The situation is worse when the parameters do not have physical descriptions [20]. The Exp-Ln model includes only three material parameters, which reduces the possibility of the existence of several optimal sets. On the other hand, the roles of parameters are completely independent (for more detailed discussions, one may refer to [16]). Therefore, performing the fitting process by using several algorithms, start points and different levels of accuracy for acquiring any other parameters set, no other optimal set was found.

Owing to the symmetry, only one quarter of the sheet is modeled. The finite element mesh is constructed with 4-node bilinear plane stress quadrilateral elements (CPS4) in ABAQUS as shown in Fig. 3. The analysis is continued until the maximum principal strain achieves the breakage value ($\varepsilon_{break}$). Though there is a full 3D strain state at the critical points, the maximum principal strain at critical points is not allowed to go beyond $\varepsilon_{break}$. It is obviously not an accurate method for anticipating the failure but estimation.

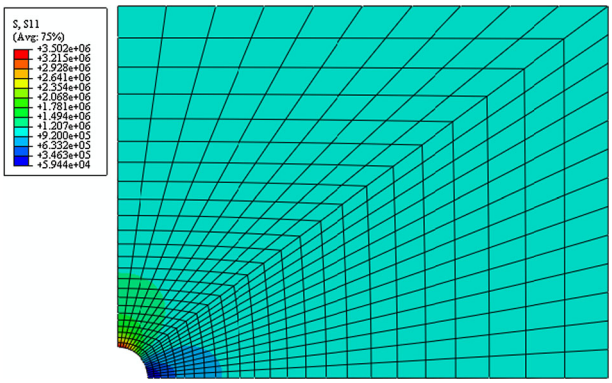


**Fig. 3** The finite element mesh used in the numerical simulations

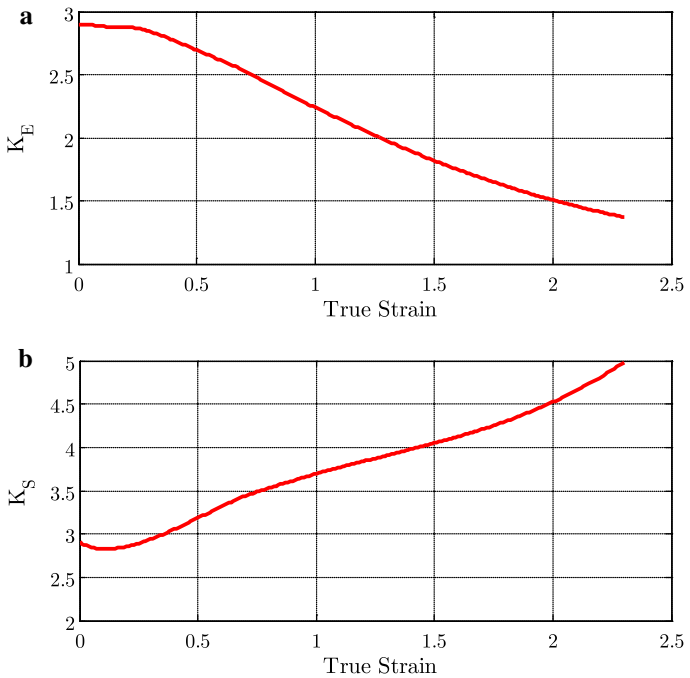


**Fig. 4** Variations of **a** the strain and **b** stress concentration factors for the unfilled NR

The strain and stress concentration factors for the unfilled NR are shown in Fig. 4a, b. We note that at small deformations both factors have the calculated value from the elasticity theory (i.e., 2.85). These values are equal because of the approximately linear behavior of the material at small deformations.

As shown in Fig. 4a, by an increasing amount of the applied deformation, $K_E$ reduces monotonically. This reduction is due to the local alignment of the material molecular chains at the critical area (around point P) which leads to a local stiffening. This phenomenon prevents straining of the material at this area, while far-field areas show less resistance to the deformation. It is to be noted that, in reality, stretches in mechanical parts hardly reach the considered large values. However, investigating variations of the concentration factors even in such extreme values is of great importance from scientific view.

In Fig. 4b, it is shown that $K_S$ exhibits a small drop followed by a sharp raise. The drop is due to the decrease in $K_E$, whereas the alignment of the chains has not been completed at the critical area, yet. A further increase in the applied deformation results in more alignment of the molecular chains which leads to more stiffening and finally to strain-induced crystallization of the material at the critical area. Onset of crystallites

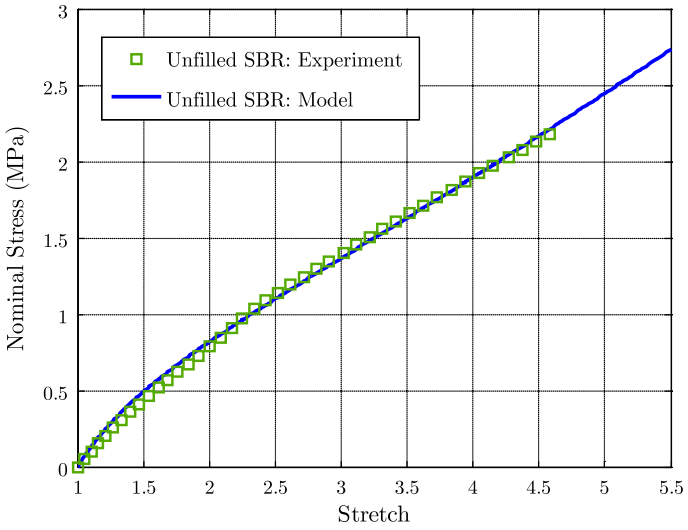


**Fig. 5** Stress–strain curve of the unfilled SBR in uniaxial tension

raises the material stiffness locally, while far-field points have not been crystallized yet. Therefore, a sharp raise of $K_S$ is observed for unfilled NR at large deformations.

Generally in FEM analysis for problems involving stress concentrations, refining the mesh makes the Gauss points closer to the edges and it affects the numerical values of strain and stress components. Refined meshes (compared to those shown in Fig. 3) were tried, and it was observed that the changes in strain and stress components were not so notable to change the trend of the concentration factors. Consequently, the mesh size slightly alters the results quantitatively but not qualitatively. In the following sections, it will be shown that type of material, amount of filler content and rate of deformation have more remarkable effects on the numerical values of the concentration factors. Thus, the trends of these factors should be more focused than their exact numerical values.

Since strain-induced crystallization occurs only in certain elastomers, it is important to investigate the variation of $K_E(K_S)$ in non-crystallizing elastomers, too. Styrene–butadiene rubber (SBR) is a synthetic non-crystallizing rubber which is used extensively in several applications due to its peculiar properties such as good abrasion resistance [21]. The experimental stress–strain curve obtained from a uniaxial tensile test is shown in Fig. 5 for an unfilled SBR along with the fitted curve of Exp-Ln model. The material parameters for this material are reported in Table 3.

The same numerical analysis is done on the unfilled SBR. Because of relatively low breakage strain for the unfilled SBR, the analysis could be done for a narrower range of strain. The results are shown in Fig. 6 where it is observed that $K_E$ and $K_S$ have a same value (equal to the result of the elasticity theory) at small deformations. $K_E$ reduces monotonically with a similar manner to the unfilled NR. $K_S$ experiences a small drop due to the decrease in $K_E$ followed by a raise due to the local alignment of the molecular chains at the critical area. The remarkable point is that, because of the non-crystallizing nature of SBR, further raise of $K_S$ is not expected by more increase in the applied deformation. Therefore, more or less all regions of the sample stiffen due to the molecular chains alignment, and so, $K_S$ finally decreases.

## 3 Effect of fillers on the strain and stress concentrations

Filler particles are generally added to elastomers in order to improve the mechanical properties of these materials. The reinforcement of elastomers by fillers has been extensively studied based on continuum mechanics as well as micromechanics [22–24]. Though type and degree of reinforcement substantially depend on the properties of filler particles (e.g., chemical composition, size and shape of particles, surface area, and reaction agents on particles) and the gum, adding fillers usually increases elastomers stiffness, tensile strength, tear strength and wear resistance [25]. For example, adding 40 phr carbon black to NR can cause an increase in shear strength and tensile strength by as much as tenfold [1].

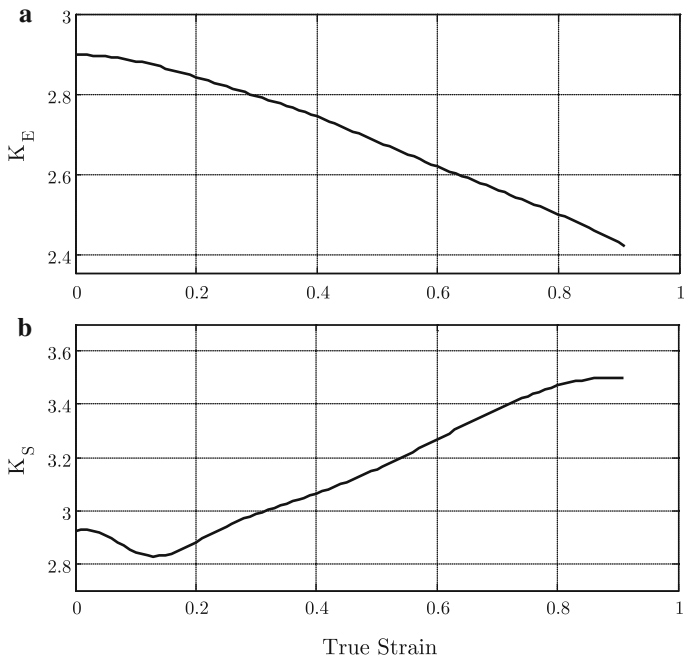


**Fig. 6** Variations of **a** the strain and **b** stress concentration factors for the unfilled SBR

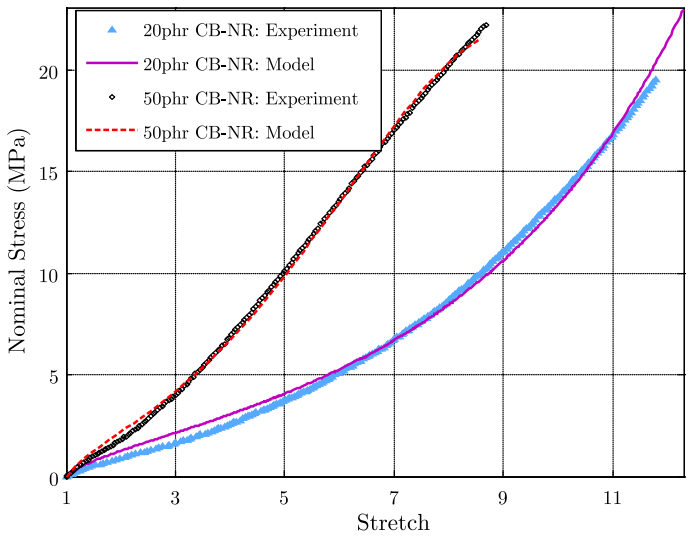


**Fig. 7** Stress–strain curves of the filled NRs in uniaxial tension

Filler particles can bond with elastomeric chains and act as cross-links. Therefore, by reinforcement of elastomers, the density of molecular chain segments in unit volume increases, whereas the average length of the segments decreases; thus, the physical parameters of the material molecular network are altered by adding fillers. Furthermore, filler particles may bond to each other physically (and even sometimes chemically) to form aggregates and agglomerates. Formation of the filler network in the material can alter the mechanical properties of the material significantly [26].

Regarding the aforementioned issues, one may expect a remarkable effect of filler content on the strain and stress distribution and consequently dependence of $K_E$ and $K_S$ on type and amount of added filler particles. To examine the effect of filler particles on $K_E$ and $K_S$, the analysis is repeated for NR containing 20 and 50 phr carbon black (CB). Uniaxial tensile tests are conducted on the filled samples (Fig. 7) to determine the breakage strain and also the material parameters as reported in Table 2.

**Table 2** Material parameters of the NRs

| | $A$[MPa] | $a[-]$ | $b[-]$ | $\varepsilon_{break}$ (%) |
|---|---|---|---|---|
| Unfilled NR | 0.152 | 0.0044 | 0.05 | 1430 |
| 20-phr CB–NR | 0.404 | 0.0063 | 0.04 | 1080 |
| 50-phr CB–NR | 0.691 | 0.012 | 0.03 | 760 |

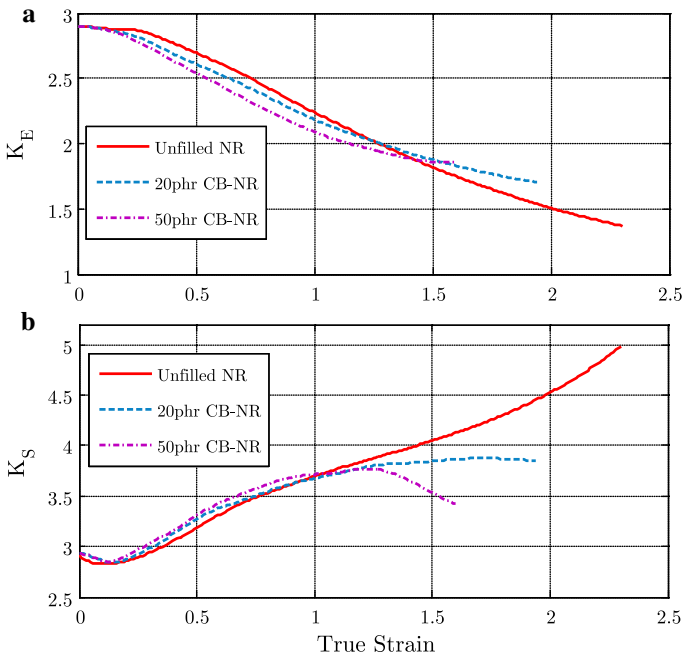


**Fig. 8** Variations of **a** the strain and **b** stress concentration factors for the filled NRs

Elastomers exhibit a stress softening phenomenon called Mullins effect, in first cycles of loading. This phenomenon has been studied extensively [27–30] and is more pronounced in filled elastomers rather than in unfilled ones. We study the first cycle of loadings for our filled samples because the worst situation of the stress concentration would occur in the first cycle. It means that, in the subsequent cycles, the stress concentration will be equal to or less than the first cycle. It should be noted that, due to the Mullins-softening, the molecular network of the material undergoes significant alterations which would affect the material parameters of any hyperelastic model used in fitting the experimental data. The constitutive models with parameters built based on the physical properties of the material molecular network (e.g., Arruda–Boyce, Gent and Exp-Ln models) have the advantage of predictability for alteration of their parameters during the network alteration. One may refer to [28,31] and references therein for more detailed discussions on the evolutions of the material parameters due to the Mullins-induced network alterations.

Results of the analysis for variations of $K_E$ and $K_S$ with respect to the applied deformation are shown in Fig. 8 in comparison with the results for the unfilled NR. It is observed that, at small deformations, the filler particles have no notable effect on the strain and stress concentration factors because the material is in the linear regime; thus, the filler network and also interactions of the filler particles with the rubbery chains are not so affected. By increasing the deformation, $K_E$ decreases for the filled samples as occurred for the unfilled material. The rate of this decrease depends on the amount of the filler content. As discussed before, interaction of filler particles with rubbery chains reduces the average length of chain segments and consequently their limiting extensibility. This phenomenon causes the local stiffening of the critical area to occur in a lower level of deformation. The early local stiffening resists against straining the critical area, and as a result, $K_E$ decreases more rapidly for the filled samples. Furthermore, the existence of the filler particles confines slippage of the chains through physical entanglements which may lead to locking of some entanglements. Wherever the level of deformations is higher, more entanglements get locked. This locking is another source of the local stiffening at the critical areas which experience higher levels of deformation compared with the far-field points.

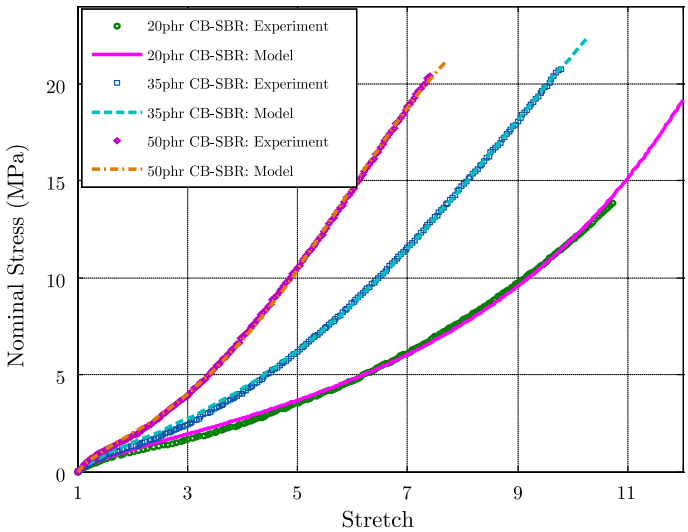


**Fig. 9** Stress–strain curves of the filled SBRs in uniaxial tension

**Table 3** Material parameters of the SBRs

| | $A$[MPa] | $a[-]$ | $b[-]$ | $\varepsilon_{break}$ (%) |
|---|---|---|---|---|
| Unfilled SBR | 0.232 | 0.0027 | 0.01 | 360 |
| 20-phr CB–SBR | 0.321 | 0.0065 | 0.008 | 970 |
| 35-phr CB–SBR | 0.451 | 0.0107 | 0.005 | 880 |
| 50-phr CB–SBR | 0.695 | 0.0131 | 0.003 | 640 |

At large deformations where the strain-induced crystallization occurs in the unfilled NR [32], the filler particles prevent the complete alignment of the chains in the filled NRs. So, the amount of the crystallization (i.e., the rapid local stiffening) is reduced significantly for these materials. Thus, in this regime, $K_E$ is slightly higher for the filled NRs rather than for the unfilled one.

At small and moderate deformations, the variation of $K_S$ for the filled samples is similar to the unfilled material, but the lower limiting chain extensibility of the filled NR causes $K_S$ to be higher (despite lower $K_E$) compared to the unfilled NR.

At large deformations, the filler particles prevent the material from crystallizing. By reaching the strain at far-field areas to its limiting value, more or less stiffening occurs at all regions and $K_S$ does not increase anymore. It is concluded that the existence of the filler particles confines $K_S$ at large deformations.

To investigate the effect of fillers on strain and stress distributions in non-crystallizing elastomers, the analysis is repeated for SBR containing 20, 35 and 50 phr carbon black content. As shown in Fig. 9, uniaxial tensile tests and fitting the experimental stress–strain curves are conducted to determine the breakage strains and also the material parameters (as depicted in Table 3).

Addition of carbon black to SBR increases the breakage strain of the material [33]. This phenomenon allows us to perform the analysis in a wider range of strain for the filled SBRs compared with the unfilled SBR where results of the numerical simulations are shown in Fig. 10.

As observed, $K_E$ has a same value for all samples at small strains (i.e., in the linear regime) but decreases by increasing amount of the deformation where the rate of decrease is higher for samples with higher filler contents. In contrast to NR, at large deformations, due to the non-crystallizing nature of SBR, the higher the filler content, the lower $K_E$.

At small and moderate deformations, variations of $K_S$ for the filled SBRs are similar to the filled NRs, but at large deformations, since no crystallization occurs in the SBRs, $K_S$ is confined for these materials. A notable point is that an increase in the filler content leads to earlier drop of $K_S$. The higher the filler content, the lower the average length of the molecular chains (and lower the limiting chain extensibility); hence, at relatively lower strains, approximately all points achieve their limiting strain. This phenomenon causes uniform stiffening at all points, and consequently $K_S$ decreases.

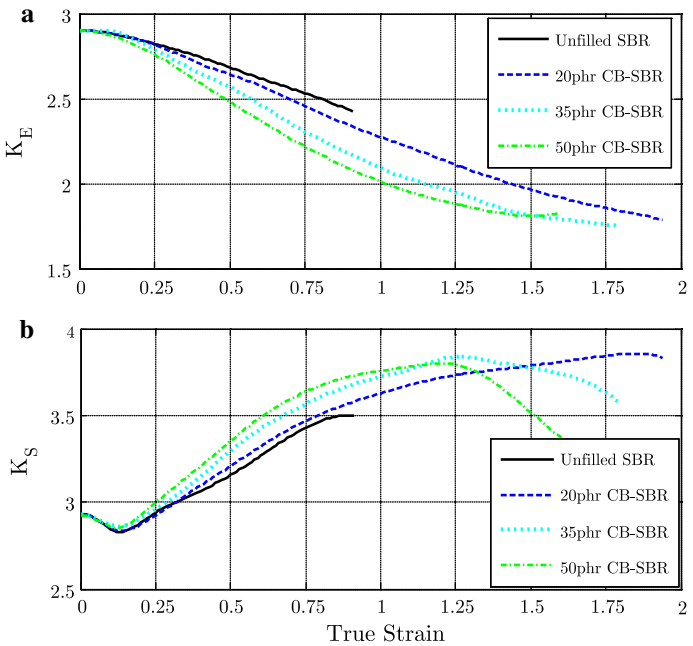


**Fig. 10** Variations of **a** the strain and **b** stress concentration factors for the filled SBRs

## 4 Effect of rate of deformation on the strain and stress concentrations

Long molecular chains of elastomers slide through each other during deformation. Readjustments, convolutions and uncoiling of the chains take place during time and cause the material to exhibit a time-dependent (i.e., strain rate-dependent) behavior [34]. This aspect of elastomer behavior has been studied extensively by visco-hyperelastic material models [35–38].

Due to the rate-dependent characteristic behavior of these materials, one may deduce that strain and stress distributions in elastomeric materials would also depend on the rate of deformations. To investigate the effect of the strain rate on the strain and stress concentrations, the stretching of the rectangular sheet with central circular hole is simulated for another unfilled SBR at different strain rates. Hoo Fatt et al. [39] conducted uniaxial tensile tests on this material. They used a tensile impact apparatus for stretching the material and reported the stress–strain curves in 76–450 $s^{-1}$ strain rates in addition to the quasi-static curve.

The equilibrium material parameters are determined from fitting the experimental quasi-static curve by the Exp-Ln hyperelastic model. To determine the viscous material parameters, the visco-hyperelastic constitutive model proposed in [40] is employed and the parameters are reported in Table 4. This three-dimensional nonlinear model utilizes a hyperelastic spring parallel to a Maxwell element as rheological model of the elastomeric materials. Also, because of the similar nature of the equilibrium and the viscous responses, the Exp-Ln strain energy function has also been used for the spring of the viscous element ($W^v$) in the model [41,42]:

$$W^v = \tilde{A}\left[\frac{1}{\tilde{a}}\exp(\tilde{a}(I_1-3)) + \tilde{b}(I_1-2)(1-\ln(I_1-2)) - \frac{1}{\tilde{a}} - \tilde{b}\right] \tag{9}$$

where $\tilde{A}$, $\tilde{a}$ and $\tilde{b}$ are viscous parameters of the material. Therefore, the total Cauchy stress is obtained as follows:

$$\boldsymbol{\sigma} = \boldsymbol{\sigma}^{equ} + \boldsymbol{\sigma}^{vis} = -p^e\mathbf{I} + 2\left(\frac{\partial W^e}{\partial I_1} + I_1\frac{\partial W^e}{\partial I_2}\right)\mathbf{B} - 2\frac{\partial W^e}{\partial I_2}\mathbf{B}^2$$
$$-p^v\mathbf{I} + \int_{-\infty}^{t}\frac{\partial}{\partial\tau}\left[2\left(\frac{\partial W^v}{\partial I_1} + I_1\frac{\partial W^v}{\partial I_2}\right)\mathbf{B} - 2\frac{\partial W^v}{\partial I_2}\mathbf{B}^2\right]\exp\left(-\frac{t-\tau}{\Theta}\right)d\tau \tag{10}$$

**Table 4** Material parameters of the unfilled SBR

| Material parameters | Equilibrium parameters | | | Viscous parameters | | | | |
|---|---|---|---|---|---|---|---|---|
| | $A$[MPa] | $a$[−] | $b$[−] | $\tilde{A}$[MPa] | $\tilde{a}$[−] | $\tilde{b}$[−] | $\varphi_{ref}$(s) | $\eta$ |
| | 0.22 | 0.006 | 0.0184 | 2.5 | 0.016 | 0.0 | 0.0058 | 0.25 |

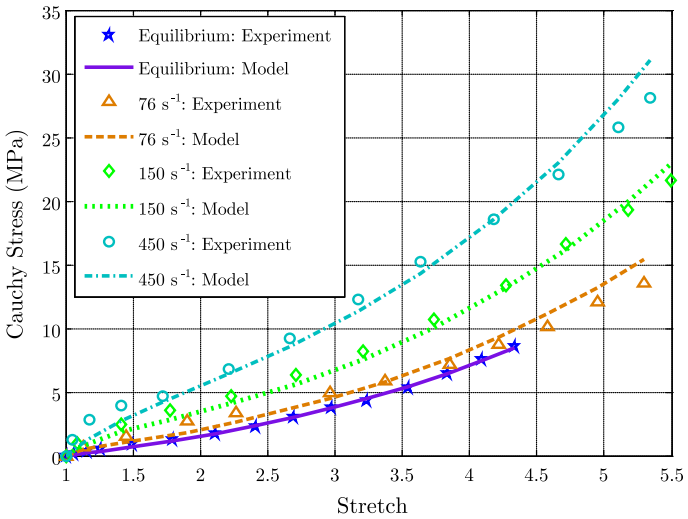


**Fig. 11** Stress–strain curves of the unfilled SBR in uniaxial tension at different strain rates

where $p^v$ is a hydrostatic pressure associated with the viscous response, and $\Theta$ is the relaxation time of the material. Furthermore, concluded from the physics of the time-dependent mechanisms, a rate-dependent relaxation time has been introduced to reduce the number of required material parameters and to avoid the complex calibration process of several relaxation times [40]:

$$\Theta = \Theta\left(\|\dot{\mathbf{C}}\|\right) = \varphi_{ref}\,\|\dot{\mathbf{C}}\|^{-\eta} \tag{11}$$

where $\varphi_{ref}$ and $\eta$ are material parameters and $\|\dot{\mathbf{C}}\| = \sqrt{\dot{C}_{ij}\dot{C}_{ij}}$ is the magnitude of the time rate of the right Cauchy–Green deformation tensor $\mathbf{C}$.

Results of the visco-hyperelastic model are shown in Fig. 11 in comparison with the experimental data at strain rates of $0\,s^{-1}$ (quasi-static), $76\,s^{-1}$, $150\,s^{-1}$ and $450\,s^{-1}$.

The numerical simulations are performed in quasi-static mode as well as $76\,s^{-1}$, $150\,s^{-1}$ and $450\,s^{-1}$ strain rates using the user-defined material subroutine (VUMAT) introduced by Khajehsaeid et al. [41]. Variations of $K_E$ and $K_S$ with respect to the applied deformation are shown in Fig. 12 at different strain rates.

The variation of $K_E$ for the equilibrium simulation is similar to that presented in Sect. 2. In the dynamic simulations, $K_E$ decreases more rapidly rather than the equilibrium simulation. As mentioned before, during deformation the molecular chains slip through each other and also through entanglements. When the deformation is quite slow, there is enough time for slippage mechanisms to take place, but in the case of fast deformations, some entanglements lock and prevent the chains from slippage. As faster as the deformation, more entanglements would lock due to the insufficient time for the slippage mechanisms. Since the amount of the deformation and also its rate is higher in the critical areas, more entanglements lock there; hence, in the dynamic deformations more stiffening occurs in these areas and it leads to faster decrease in $K_E$ in comparison with the equilibrium deformation (as high as the deformation rate, faster decrease is observed for $K_E$). At large stretches, since the chains of all areas achieve their limiting extensibility and also locking of the entanglements occurs almost uniformly, more or less all areas stiffen and this prevents more decrease in $K_E$. A notable point is that, as high as the deformation rate, the universal stiffening occurs at lower strains.

The stress concentration factor has the same value for all rates at small deformations, but by increasing amount of the applied deformation $K_S$ increases despite the reduction in $K_E$. It is due to the increase in stiffness of the critical areas. The increase in $K_S$ is more rapid for faster deformations where more locking

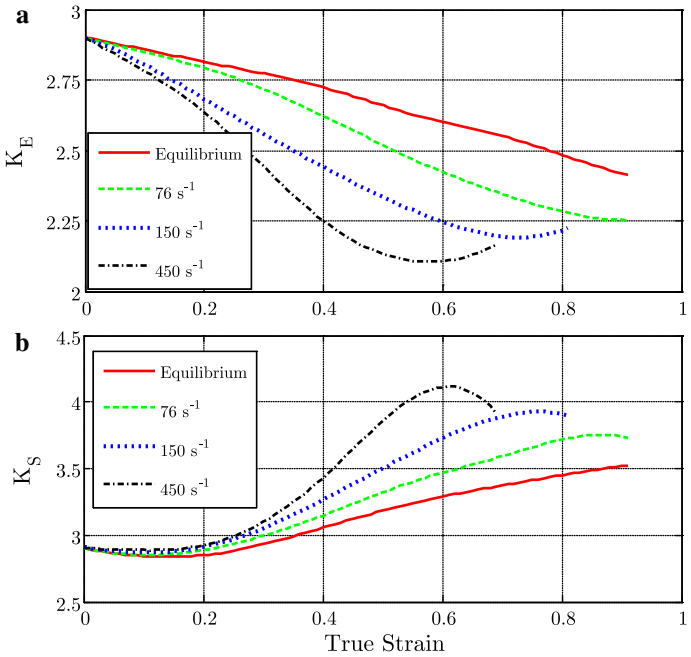


**Fig. 12** Variations of **a** the strain and **b** stress concentration factors for the unfilled SBR at different strain rates

occurs. Finally, at large stretches, when the uniform stiffening takes place, $K_S$ does not increase anymore and even decreases at high strain rates.

## 5 Summary and conclusions

Strain and stress concentrations were studied for elastomers at finite deformations. As a typical problem of strain and stress localizations, the investigations focused on elastomeric rectangular sheets with circular hole at the center. The problem was simulated numerically using the material parameters obtained from experimental tests conducted on 0, 20, 50 phr carbon black-filled NR and 0, 20, 35, 50 phr carbon black-filled SBR. It was observed for all samples that at small strains (because of the linear behavior of the materials) the strain and stress concentration factors have the same value which is equal to the result of the elasticity theory. For the unfilled samples, it was shown that the strain concentration factor $K_E$ decreases monotonically by increasing the applied deformation where the stress concentration factor $K_S$ rises sharply after a small drop. The raise of $K_S$ was sharper for NR as a crystallizing rubber (up to $K_S = 5$) compared to SBR as a non-crystallizing rubber (up to $K_S = 3.5$) because the strain-induced crystallization resulted from the alignment of molecular chains in NR.

The effect of filler reinforcement on strain and stress concentrations was also analyzed. At small deformations, filler particles had no notable effect on $K_E$ and $K_S$. By increasing amount of the deformation, the reduction in $K_E$ became faster as the filler content increased. At large deformations, because of filler's prevention of chains complete alignment (which can lead to crystallization), $K_E$ was higher for filled NRs compared to the unfilled NR. But it was not the case for SBR because crystallization does not occur in SBR at all. The presence of filler particles slightly raised $K_S$ at moderate strains, but at large strains, in the case of NR, the fillers reduced $K_S$ significantly, while in the case of SBR the fillers only shifted the maximum value of $K_S$ to a lower level of strain.

To investigate the effect of deformation rate, the problem was simulated for an unfilled SBR at different strain rates. A visco-hyperelastic constitutive law along with an associated user-defined material subroutine (VUMAT) in ABAQUS/Explicit was employed in the simulations. It was observed that increasing the rate of deformation lowers $K_E$ due to the locking of physical entanglements at the critical areas. However, at higher rates of deformations $K_S$ was higher despite the reduction in $K_E$.

It is concluded that, at finite deformations, the strain and stress concentration factors vary with the amount of the applied deformation. Particularly, in the case of crystallizing elastomers, the stress concentration factor

can rise from its theoretical value remarkably which should be noticed in design purposes. Addition of carbon black is recommended particularly for crystallizing elastomers because it prevents $K_S$ from growing when the strains get larger. Furthermore, we conclude that due to the locking of entanglements, increasing the rate of deformation concentrates stress substantially which is not desired in the design of mechanical parts. Though the studied problem is a special case of strain and stress concentrations, the suggested physical explanations might also hold for other problems involving strain and stress localizations in elastomers.

## References


1. Mark, J.E., Erman, B., Eirich, F.R.: The Science and Technology of Rubber. Academic Press, New York (2005)
2. Ward, I.M., Sweeney, J.: An Introduction to the Mechanical Properties of Solid Polymers. Wiley, New York (2004)
3. Lindley, P.B.: Strain concentrations at the corners of stretched rubber sheets. J. Strain Anal. Eng. Des. **6**, 279–285 (1971)
4. Kadlowec, J., Wineman, A., Hulbert, G.: Elastomer bushing response: experiments and finite element modeling. Acta Mech. **163**, 25–38 (2003)
5. Walter, D.P., Pilkey, D.: Peterson's Stress Concentration Factors, 3rd edn. Wiley, New York (2008)
6. Elmukashfi, E., Kroon, M.: Numerical analysis of dynamic crack propagation in biaxially strained rubber sheets. Eng. Fract. Mech. **124–125**, 1–17 (2014)
7. Yang, Z., Kim, C.-B., Cho, C., Beom, H.G.: The concentration of stress and strain in finite thickness elastic plate containing a circular hole. Int. J. Solids Struct. **45**, 713–731 (2008)
8. Yang, Z.: Stress and strain concentration factors for tension bars of circular cross-section with semicircular groove. Eng. Fract. Mech. **76**, 1683–1690 (2009)
9. Fukahori, Y., Seki, W.: Stress analysis of elastomeric materials at large extensions using the finite element method. J. Mater. Sci. **28**, 4471–4482 (1993)
10. Troyani, N., Gomes, C., Sterlacci, G.: Theoretical stress concentration factors for short rectangular plates with centered circular holes. J. Mech. Des. **124**, 126–128 (2002)
11. Troyani, N., Sterlacci, G., Gomes, C.: Simultaneous considerations of length and boundary conditions on theoretical stress concentration factors. Int. J. Fatigue **25**, 353–355 (2003)
12. Timoshenko, S., Goodier, J.N.: Theory of Elasticity. McGraw-Hill Book Company, New York (1970)
13. Darijani, H., Naghdabadi, R.: Hyperelastic materials behavior modeling using consistent strain energy density functions. Acta Mech. **213**, 235–254 (2010)
14. Arruda, E.M., Boyce, M.C.: A three-dimensional constitutive model for the large stretch behavior of rubber elastic materials. J. Mech. Phys. Solids **41**, 389–412 (1993)
15. Pucci, E., Saccomandi, G.: A note on the Gent model for rubber-like materials. Rubber Chem. Technol. **75**, 839–851 (2002)
16. Khajehsaeid, H., Arghavani, J., Naghdabadi, R.: A hyperelastic constitutive model for rubber-like materials. Eur. J. Mech. A Solids **38**, 144–151 (2013)
17. Khajehsaeid, H., Naghdabadi, R., Arghavani, J.: A strain energy function for rubber-like materials. Const. Models Rubber **8**, 205–210 (2013)
18. Khajehsaeid, H., Rabiei, S.: Effect of intermolecular forces in mechanical behavior of elastomers. In: Proceedings of the Society of Engineering Science 51st Annual Technical Meeting, West Lafayette, Purdue University October 1–3, 2014. Purdue University Libraries Scholarly Publishing Services
19. Rivlin, R.S., Saunders, D.W.: Large elastic deformations of isotropic materials. VII. Experiments on the deformation of rubber. Philos. Trans. R. Soc. Lond. Ser. A Math. Phys. Sci. **243**, 251–288 (1951)
20. Ogden, R., Saccomandi, G., Sgura, I.: Fitting hyperelastic models to experimental data. Comput. Mech. **34**, 484–502 (2004)
21. Pal, K., Rajasekar, R., Kang, D.J., Zhang, Z.X., Pal, S.K., Das, C.K., Kim, J.K.: Effect of fillers on natural rubber/high styrene rubber blends with nano silica: morphology and wear. Mater. Des. **31**, 677–686 (2010)
22. Dannenberg, E.: The effects of surface chemical interactions on the properties of filler-reinforced rubbers. Rubber Chem. Technol. **48**, 410–444 (1975)
23. Berriot, J., Lequeux, F., Monnerie, L., Montes, H., Long, D., Sotta, P.: Filler-elastomer interaction in model filled rubbers, a 1H NMR study. J. Non Cryst. Solids **307**, 719–724 (2002)
24. Leblanc, J.L.: Rubber-filler interactions and rheological properties in filled compounds. Prog. Polym. Sci. **27**, 627–687 (2002)
25. Tangudom, P., Thongsang, S., Sombatsompop, N.: Cure and mechanical properties and abrasive wear behavior of natural rubber, styrene-butadiene rubber and their blends reinforced with silica hybrid fillers. Mater. Des. **53**, 856–864 (2014)
26. Fritzsche, J., Klüppel, M.: Structural dynamics and interfacial properties of filler-reinforced elastomers. J. Phys. Condens. Matter **23**, 1–11 (2011)
27. Horgan, C.O., Ogden, R.W., Saccomandi, G.: A theory of stress softening of elastomers based on finite chain extensibility. Proc. R. Soc. Lond. Ser. A Math. Phys. Eng. Sci. **460**, 1737–1754 (2004)
28. Marckmann, G., Verron, E., Gornet, L., Chagnon, G., Charrier, P., Fort, P.: A theory of network alteration for the Mullins effect. J. Mech. Phys. Solids **50**, 2011–2028 (2002)
29. Bueche, F.: Molecular basis for the Mullins effect. J. Appl. Polym. Sci. **4**, 107–114 (1960)
30. Diani, J., Fayolle, B., Gilormini, P.: A review on the Mullins effect. Eur. Polym. J. **45**, 601–612 (2009)
31. Khajehsaeid, H.: Development of a network alteration theory for the Mullins-softening of filled elastomers based on the morphology of filler-chain interactions. Int. J. Solids Struct. **80**, 158–167 (2016)

32. Negahban, M.: Modeling the thermomechanical effects of crystallization in natural rubber: I. The theoretical structure. Int. J. Solids Struct. **37**, 2777–2789 (2000)
33. Fukahori, Y.: The mechanics and mechanism of the carbon black reinforcement of elastomers. Rubber Chem. Technol. **76**, 548–566 (2003)
34. Hoo Fatt, M.S., Ouyang, X.: Integral-based constitutive equation for rubber at high strain rates. Int. J. Solids Struct. **44**, 6491–6506 (2007)
35. Amin, A.F.M.S., Lion, A., Sekita, S., Okui, Y.: Nonlinear dependence of viscosity in modeling the rate-dependent response of natural and high damping rubbers in compression and shear: Experimental identification and numerical verification. Int. J. Plast. **22**, 1610–1657 (2006)
36. Bergström, J., Boyce, M.: Constitutive modeling of the time-dependent and cyclic loading of elastomers and application to soft biological tissues. Mech. Mater. **33**, 523–530 (2001)
37. Reese, S.: A micromechanically motivated material model for the thermo-viscoelastic material behaviour of rubber-like polymers. Int. J. Plast. **19**, 909–940 (2003)
38. Anani, Y., Alizadeh, Y.: Visco-hyperelastic constitutive law for modeling of foam's behavior. Mater. Des. **32**, 2940–2948 (2011)
39. Hoo Fatt, M.S., Ouyang, X.: Three-dimensional constitutive equations for Styrene Butadiene rubber at high strain rates. Mech. Mater. **40**, 1–16 (2008)
40. Khajehsaeid, H., Arghavani, J., Naghdabadi, R., Sohrabpour, S.: A visco-hyperelastic constitutive model for rubber-like materials: a rate-dependent relaxation time scheme. Int. J. Eng. Sci. **79**, 44–58 (2014)
41. Khajehsaeid, H., Baghani, M., Naghdabadi, R.: Finite strain numerical analysis of elastomeric bushings under multi-axial loadings: a compressible visco-hyperelastic approach. Int. J. Mech. Mater. Des. **9**, 385–399 (2013)
42. Khajehsaeid, H., Ramezani, M.A.: Visco-hyperelastic modeling of automotive elastomeric bushings with emphasis on the coupling effect of axial and torsional deformations. In: Proceedings of the Society of Engineering Science 51st Annual Technical Meeting, West Lafayette, Purdue University October 1–3, 2014. Purdue University Libraries Scholarly Publishing Services